

Gravitational collisions in cosmological N -body codes

I. Suisalu^{1,2,3*} and E. Saar^{1,3†}

¹ *Tartu Astrophysical Observatory, Tõravere, EE-2444, Estonia*

² *Royal Observatory Edinburgh, Blackford Hill, Edinburgh EH9 3HJ, U.K.*

³ *Theoretical Astrophysics Center, Blegdamsvej 17, Copenhagen, DK-2100, Denmark*

3 October 2018

ABSTRACT

We study the accumulation of errors in cosmological N -body algorithms that are caused by representing the continuous distribution of matter by massive particles, comparing the P³M and Adaptive Multigrid codes. We use for this a new measure of two-body relaxation suitable for nonstationary gravitating systems. This measure is based on accumulated deflection angles of particle orbits and it does not saturate during evolution. We have found that the role of gravitational collisions in standard P³M-models is rather high, and in order to avoid collision effects we recommend to use comoving softening parameters $\varepsilon \geq 1.0$ (in grid units).

Key words: gravitation – methods:numerical – dark matter – large-scale structure of Universe

1 INTRODUCTION

Cosmological simulations use N -body algorithms that replace the initially continuous distribution of (dark) matter by discrete and rather massive ‘particles’. This helps to simulate intersecting streams of collisionless matter that are common at the time of formation of cosmological structure. Interactions between these particles may, however, differ from the dynamics of the continuous media they are meant to approximate. The main source of discrepancy are close encounters between the particles (gravitational collisions).

The popular belief has been that if the number of points in the simulation is sufficiently large, the discreteness effects (gravitational collisions or close encounters between mass points) do not play an important role. These effects have been studied only for tree-codes in case of stationary gravitating systems (Hernquist & Barnes 1990, Huang, Dubinski & Carlberg 1993). We shall describe in this paper the role of gravitational collisions in high-resolution cosmological codes.

Among the different N -body algorithms used for cosmological simulations the P³M (Particle-Particle-Particle-Mesh) algorithm has become the industry standard for high-resolution simulations. It was designed initially for plasma physics simulations and ported to cosmology by Efstathiou & Eastwood (1981). It has been clearly documented in textbooks (Hockney & Eastwood, 1988, Couchman, 1995) and the code is practically in public domain. This code was the first candidate for our study.

The P³M-code improves considerably the resolution of a standard PM (Particle-Mesh) code by splitting forces in two parts – the long-range force from the overall density distribution on a mesh and the short-range force from nearest neighbours, calculating the latter by summation over pairs of particles. The algorithm was devised initially to simulate collections of pointlike particles. In cosmological simulations of formation of structure the basic dark matter density is smooth and does not lend itself easily to representation by discrete mass points. This difficulty is usually alleviated by introducing smoothing parameters in pairwise forces, effectively replacing the mass points by extended spherical clouds.

In order to study discreteness properties of the P³M-code one should have smooth codes with spatial resolution comparable to the P³M. Such codes have appeared only recently, and most of them are grid-based multi-resolution schemes (except that of Pen (1994) that uses a global deformed grid). These codes improve the spatial resolution in selected regions (mostly in those of high density). We shall describe these codes and their main differences below; for comparison we used our adaptive multigrid code (Suisalu & Saar 1995).

We ran also one simulation using the popular tree-code (Barnes & Hut 1986). Its deflection properties have been studied before (Hernquist & Barnes 1990, Huang et al. 1993), but for a stationary case only.

The usual tool to measure pairwise collisions is the study of energy diffusion (see the studies of three-code simulations cited above). This is proper for stationary gravitating systems, where energy is otherwise conserved and heating comes only from pairwise interactions; in cosmology the

* E-mail: ivar@aai.ee

† E-mail: saar@aai.ee

overall energy changes with time and it is not the best measure for collisions. We propose instead of it to study orbital deflection angles, concentrating only on the change of direction of velocities and not on the change of their absolute values.

2 SIMULATIONS

As the adaptive grid methods are not so well known as the P³M and one is forced to select between different versions, we shall describe their differences below.

All these methods form subgrids of higher spatial resolution in regions where density is higher than a prescribed limit. They use for boundary conditions on a subgrid the values of the potential (Dirichlet conditions) interpolated from the coarser grid, but they differ when finding the solutions for the potential. The problem is if the coarse grid solution should depend on the finer grid solution at the same point, or not. It certainly should if we used exact direct solvers of linear systems arising from discretized partial differential equations, but the situation is not clear for approximate iterative solvers. In cosmological simulations we do not have an exact source term, either, as our density determination may depend on a grid level.

In an ideal situation solutions of different resolution should converge rapidly during the iteration process. In practice convergence is rather slow, as solutions on coarser grids are considerably changed by temporary solutions on finer subgrids (see, e.g. Brandt 1987). This issue has been discussed by Anninos, Norman & Clarke (1994) who classify adaptive grid methods as having either one or two-way interfaces between parent and subgrids.

As an example, in the multi-grid method developed by Jessop, Duncan & Smith (1994) only one-way grid interfaces are used that implies that the local fine grid solution can be different from the coarse grid solution. They find the local solution by iteration on the subgrid only. A recent adaptive code by Splinter (1995) uses a similar methodology, although the algorithms for finding the solution on subgrids differ.

In contrast, in our AMG (Adaptive Multigrid) code (Suisalu & Saar 1995) the solution for local subgrids is obtained simultaneously with the global solution using the full multi-grid method (Brandt 1977). According to the above classification AMG uses two-way grid interfaces between finer and coarser grids, as information passes in both directions during iterations. The reason why we have been left alone in this class is that here it is harder to get good convergence of the iterative solution process. We believe that two-way interfaces, once they have been built, are closer to the exact solution, and we shall use below our AMG-code for comparison with the AP³M-code.

At first we encountered difficulties in building our models, as the natural boundary conditions for a multigrid code are the Dirichlet conditions, and our code was initially tuned for this case. In order to follow the evolution of spatially periodic P³M models we had to modify our code for periodic boundary conditions.

If we use iterative methods to solve the Poisson equation on a grid, we discover that in the case of periodic boundaries the linearized system of algebraic equations that we have to solve becomes singular. Singular systems are more difficult

Table 1. Simulation parameters

Sim.	L	N	ε	h_{min}
P3M1*	32 ³	32 ³	0.2	1
P3M2	32 ³	32 ³	1.0	1
P3M3	32 ³	32 ³	2.0	1
P3M4	32 ³	64 ³	0.2	1
APM	32 ³	32 ³	0.2 [†]	1/8
AMG1	32 ³	32 ³		1/16
AMG2	32 ³	64 ³		1/32
TREE		16440	0.2	

* Three different spectra
† Short-range accelerations excluded

to solve, and the problem becomes even harder if we consider interactions between the subgrids and the global grid. In the case of full two-way interfaces that we use, solutions on subgrids always induce changes in global solutions that violate global boundary conditions, and this requires usually additional iterations. In the periodic case the global solution is very sensitive to violations of the zero total mass condition that are generated by local subgrids, and convergence becomes very slow.

The remedy we chose was to use the Galerkin condition to modify the difference operators on coarser grids. Namely, we calculate the difference operator L^H on the coarse grid as

$$L^H = I_h^H L^h I_H^h, \quad (1)$$

where L^h is the difference operator on the fine grid, I_h^H is the restriction operator from the fine grid to the coarse grid and I_H^h is the corresponding interpolation operator. This technique helps to integrate singular systems, and it is described in detail by Hackbusch (1985). We found it essential for speeding up the convergence of the solution for the gravitational potential.

We chose to impose these conditions only when finding the solution for the global grid and did not modify the differential operator L on subgrids. In order to satisfy the boundary conditions themselves, we copied appropriately the boundary regions on global grids between iterations.

For P³M simulations we used H. Couchman's Adaptive P³M code AP³M (Couchman 1991) that speeds up the normal P³M by generating subgrids in regions of high particle density and finding there a smooth solution for the potential. This works to decrease the volume of pairwise force summation and considerably speeds up the algorithm. As concerns the adaptive smooth solution, the AP³M-method belongs to the class of those with an one-way interface.

We have run and analyzed 6 P³M simulations, 3 PM-type simulations and one tree-code simulation, their parameters are summarized in Table 1. The first column labels the simulations, L is the base mesh size in cells (the physical size is $80h^{-1}$ Mpc for all simulations), N is the number of particles used, ε is the comoving softening parameter and h_{min} the minimal meshsize for adaptive models.

Couchman (1995) advises using softening radii that are constant in physical coordinates that leads to increasing discreteness during simulations. While this could be appropriate to describe the interaction of separate mass concentra-

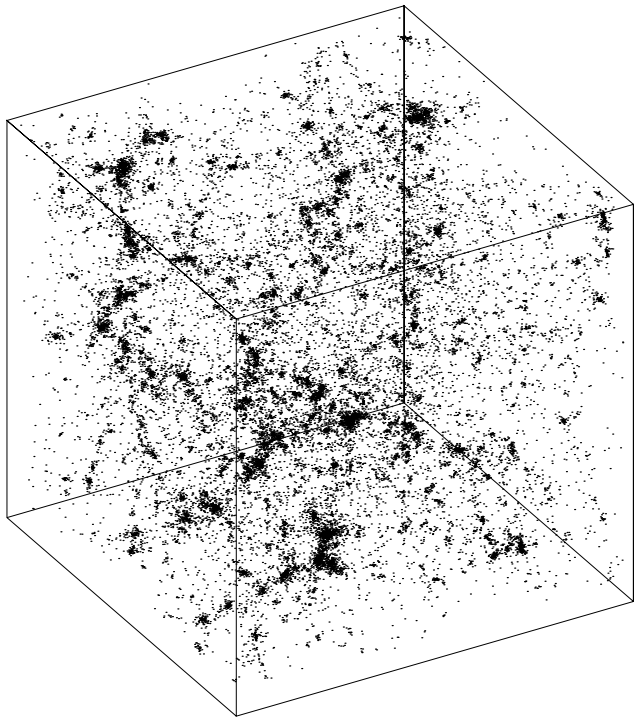


Figure 1. Particle distribution for the model P3M1 (P3M with a small softening parameter $\varepsilon = 0.2$) at the present epoch $a = 9$. The spectral index is $n = -1$ and the size of the cube is $80h^{-1}$ Mpc.

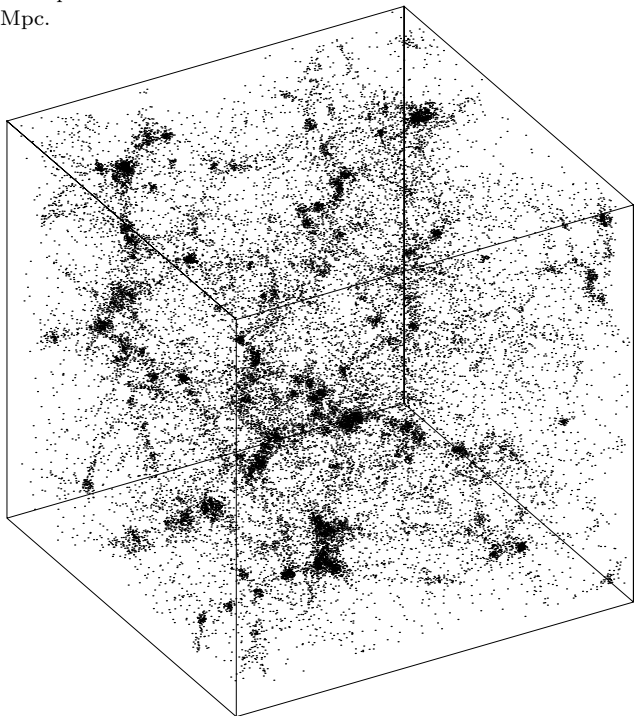


Figure 2. Particle distribution for the model AMG1 (AMG with 4 subgrid levels) at $a = 9$. The initial conditions and the cube size are the same as for the model P3M1 in Fig. 1.

tions that may form during the simulation, it is certainly not the best description for dark matter. We used comoving softening to keep P³M-simulations closer to smooth grid simulations; e.g., Gelb & Bertschinger (1994) have chosen the same approach.

Altogether we used three different values of the softening parameter $\varepsilon = 0.2, 1$ and 2 (our minimal softening

is that normally used in P³M-simulations). The maximum number of refinement levels for AP³M was 4. The model we call APM is similar to the P3M1 with the only difference that we commented out in the source code the lines that updated velocities by accelerations from short-range forces – this is essentially a PM-model with adaptive mesh refinement, hidden inside the camp of AP³M-models.

Two other PM simulations labeled AMG1 and AMG2 were run using our Adaptive Multigrid code modified for periodic boundary conditions as described above. This code gives a spatial resolution for forces similar to that of P³M codes without the need to consider pairwise forces. The last two codes differ by the number of points used and also by the number of subgrid levels allowed, 4 for AMG1 and 5 for AMG2.

The tree-code we used was the so-called ‘Barnes’ export’ code with quadrupole corrections. While the computational volume for all other models was a periodic cube with the size of $80h^{-1}$ Mpc, the volume for the tree-code was a sphere (with the same diameter). We used an opening angle $\theta = 0.8$ and physical coordinates with the timestep of 0.001 Gy.

We used the same initial conditions for all our models, trying to eliminate all possible sources of differences. The initial conditions were generated using the test power law spectrum with the spectral index $n = -1$ from the Couchman’s Adaptive P³M distribution (see Couchman 1995 for a detailed description). For the P3M1-model we generated also two other realizations with the initial spectra as power laws with indices $n = -2$ and $n = 0$. When we compare different models from the Table 1, we use always those with the $n = -1$ spectrum.

As we simulated the simple $\Omega = 1$ cosmology, we could choose our starting time at will (we use the scalefactor a as our time variable). We started at $a = 1$ and followed the evolution until $a = 9$ when $\sigma_8 \approx 1$ for all models, thus we brought our models up to the present time. In order to study the growth of orbital deflections further, we followed the evolution of selected models for longer periods, up to $a = 30$.

We did not use the usual energy condition to check our time steps. Instead of this we use in our AMG code the Courant condition:

$$v_{max}\Delta a < 0.2h_{min}, \quad (2)$$

(we change the time step when necessary, using an asymmetric leapfrog integration). As the AP³M-code uses a constant timestep, we ran first our AMG1-model, found the minimum timestep used ($\Delta a = 0.0625$) and used it for all simulations (we even ran AMG1 once more). This guarantees the use of the same algorithm for integration in time and eliminates one possible source of difference between models. The value of Δa we chose corresponds to $\Delta p = 0.01$ for the time variable $p = (3/2)a$ used in AP³M for $\Omega = 1$. This time step is much smaller than usual, but it is necessary to follow accurately particle trajectories.

The typical density distribution for our models is shown in Figs. 1 and 2. The first one shows the particle distribution for the model P3M1 at $a = 9$ and the second one a similar one for the model AMG1. The density distribution in the former seems to be more developed and has more distinct substructure, while AMG has retained more of linear structure elements and is less clumpy. We may suspect that

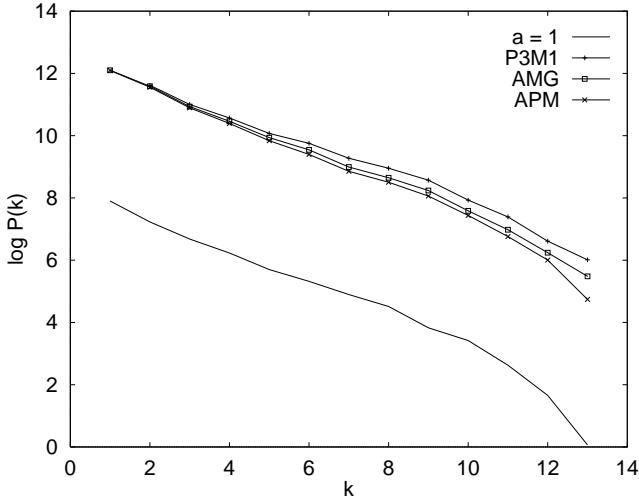


Figure 3. The evolution of the initial density power spectrum $P(k)$ (the curve marked $a = 1$) in different models. The spectra for the three models shown at the final moment $a = 9$ are labeled according to Table 1. The wavenumber k is given in the comoving grid units.

the difference is due to pairwise collisions but we cannot say this on the basis of comparing density distributions only. The overall impression of both models is rather similar, of course – they start from identical initial conditions.

The evolution of the spectrum for different models was also rather similar (see Fig. 3). The difference is in the growth of small-scale modes that is the highest for the P³M-models with a small softening (P3M1), the lowest for the APM model (this is essentially a pure PM-model) and intermediate for the smooth but high-resolution AMG1 run. The difference between the last two models can be explained by different depths of adaptive subgrid levels used (3 for APM and 4 for AMG1) and by the fact that the effective smoothing in P³M is somewhat higher than that in AMG (about 3.5 versus 2 cell sizes). This makes the resolution achieved by AMG1 about 4 times higher than that in APM.

3 DEFLECTION ANGLES

It is well known that during the linear stage of growth of density perturbations particle velocities retain their initial directions; the well-known Zeldovich approximation says

$$\mathbf{x} = \mathbf{q} + b(t)\mathbf{v}(\mathbf{q}), \quad (3)$$

where \mathbf{x} is the comoving coordinate of a particle labeled by its initial coordinates \mathbf{q} and $b(t)$ is the density growth rate from the linear theory, a function of time only. This shows clearly that while the velocity amplitude may change in time, its direction remains fixed. In fact, the components of the velocity direction are adiabatic invariants of motion in the initial stage, while particle energies change with time even without any interaction. This suggests that the change

of the velocity direction is a better measure of gravitational interaction than the usually used energy diffusion.

Nonlinear effects – growth of structure and pairwise collisions – both contribute to the change of the direction of velocity, and if we define the deflection angle $d\phi$ for a particle by

$$d\phi = |\mathbf{v} \cdot d\mathbf{v}|/v^2, \quad (4)$$

then the total angle ϕ accumulated during the run of the simulation reflects all gravitational collisions suffered by the particle. The quantity ϕ does not describe the real angle between the initial and final direction of the velocity of a particle, as it omits the other degree of freedom θ necessary to describe a direction in a 3-D space. However, in case of a small total deflection the two angles are connected by

$$\langle \sin^2 \Phi \rangle = 2/3[1 - \exp(-3S/2)] \quad (5)$$

(Standish & Aksnes 1969), where the accumulated square deflection for a trajectory S is

$$S = \sum_a (d\phi)^2 \quad (6)$$

(a is our time coordinate). The mean in (5) concerns all trajectories with the same $d\phi$ -sequence but with different θ . For small values of S it is equal to the mean square of the final deflection angle Φ , but for a long history of collisions $\langle \sin^2 \Phi \rangle$ will reach the value 2/3 that describes an isotropic distribution. On the contrary, the accumulated square deflection S does not saturate and continues to describe the total effect of gravitational interactions. In this respect it is also better than the often-used measure of orbital divergence that saturates easily for spatially limited systems.

In order to be able to catch large single deflections we computed the deflection angles in the simulations as

$$d\phi = \arccos(\mathbf{v}_t \cdot \mathbf{v}_{t+\delta t}/|\mathbf{v}_t||\mathbf{v}_{t+\delta t}|), \quad (7)$$

this did not add significantly to the cost of the simulations. We summed both the deflection angles and their squares for every trajectory during a simulation.

After this work was finished, we learned about a similar measure proposed recently by Bagla & Padmanabhan (1995) to describe nonlinearity in cosmological structure formation. They describe deviations from the linear stage by a measure

$$D_{gu} = (\mathbf{u} - \mathbf{g})^2/u^2 \quad (8)$$

(as \mathbf{u} is the velocity with respect to the dimensionless time a , its dimension is the same as that of the acceleration \mathbf{g}). Their measure is easier to calculate than ours, but it has to be modified for other cosmologies (the Zeldovich approximation gives zero for this expression only for $\Omega = 1$ universe), ours does not depend on the background cosmology. But we see clearly that there are two sources for orbital deflections – nonlinear evolution of particle orbits in the smooth background field described by (8) and the pairwise (gravitational) collisions we are looking for. Of course, both these sources contribute to the energy diffusion, too.

While deflection angles reflect histories of individual particles, the simplest characteristic describing the change of all particle trajectories in a simulation is the mean of accumulated squares of deflection angles for all trajectories (S). If particle motions are quasi-linear, as in the Zeldovich approximation, particles follow their initial direction (only

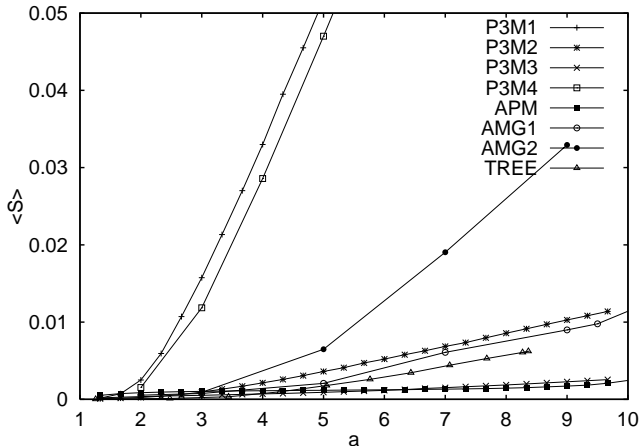


Figure 4. Growth of the mean accumulated square deflection $\langle S \rangle$ with dimensionless time a (the scale factor). The models are labeled according to Table 1; the highest growth is observed in case of the P³M-models with a normal smoothing parameter $\varepsilon = 0.2$.

their velocity may change in time) and $\langle S \rangle = 0$. Growth of the deflection angles describes nonlinear interactions, either via the mean field or by pairwise gravitational collisions.

In Fig. 4 we see the evolution of the deflection measure $\langle S \rangle$ in time for different models. First we see a striking difference between the P³M-models with different smoothing parameters; for the normally accepted smoothing parameter ($\varepsilon = 0.2$) the accumulation of deflection angles is very rapid compared to those for larger ε . Contrary to the common belief, the rate of growth of deflection angles does not depend much of the total number of particles N – compare the curves P3M1 and P3M4, the latter is for a model with 8 times more particles than the P3M1. Our multigrid models lie in the middle of the range, the model AMG1 practically coinciding with the P3M2. This is understandable, as $\varepsilon = 1$ corresponds to a cell-sized smoothing; the model P3M3 $\varepsilon = 2$ is evidently ‘oversmoothed’.

Surprisingly, the model AMG2 gives larger deflections than the AMG1. This can hardly be caused by the larger number of particles, a much more likely cause is that we have allowed an extra level of refinement in this model and follow particle trajectories better. An additional source of deflections could be the force errors that each refinement introduces near subgrid boundaries; as we have shown earlier (Suisalu and Saar 1995), these errors are usually small, less than one per cent, but in rare cases they may reach a few per cent. Similar errors are present in the AP³M-code, where the usual requirement is to limit them by 6 per cent. We stress once more that this value describes very rare errors. Anyway, such errors may get amplified in a square-weighted characteristic as $\langle S \rangle$ is. Another surprise is a relatively low deflection measure obtained for our tree-code run.

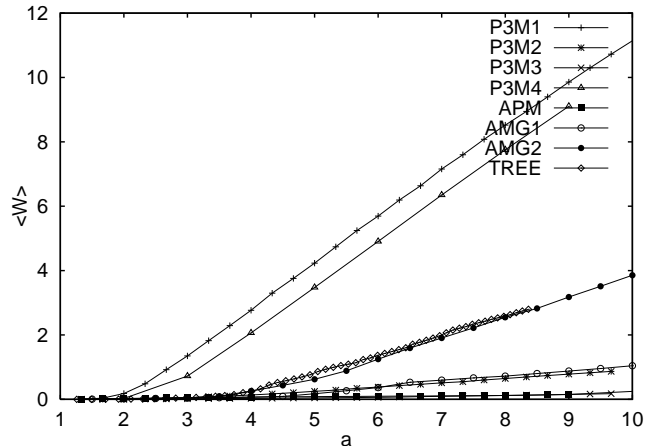


Figure 5. Growth of the mean squared angular velocity deflections $\langle W \rangle$ with dimensionless time a . The models are labeled according to Table 1; the highest growth is observed in case of the P³M-models with a normal smoothing parameter $\varepsilon = 0.2$.

As we mentioned above, the deflection may be caused both by gravitational collisions and by interactions with the mean gravitational field. It is well known that in case of uncorrelated deflections particles follow a random walk in the energy space (see, e.g., Huang et al. 1993). This would translate in our case to

$$\frac{dS}{da} = n(\Delta\phi)^2 \quad (9)$$

that would give a $\langle S \rangle \sim t$ dependence (n is here the mean frequency of collisions and $(\Delta\phi)^2$ the characteristic value of a single squared deflection). This is close to the a -dependence seen in Fig. 4.

However, in our nonstationary simulations we have to consider also the possible role of the mean-field effects. We can roughly model strong mean-field deflections, supposing that all particles rotate in circular orbits with angular velocities ω_i . In this case the computed deflection measure would grow as

$$\langle S(a) \rangle = \frac{1}{N} \sum_i^N \sum_a (\omega_i \Delta a)^2 = \frac{a \Delta a}{N} \sum_i \omega_i^2. \quad (10)$$

As we see, $\langle S \rangle$ caused by a strong mean-field interaction is also proportional to time a , as the expected effect of collisions was.

In order to differentiate between the signatures of mean-field deflections and those caused by pairwise collisions, we introduced a new (‘velocity’) deflection measure W for the growth of the squared deflections of the angular velocity of a particle:

$$W(a) = \int_{a_0}^a \left(\frac{d\phi}{da} - \omega \right)^2 da, \quad (11)$$

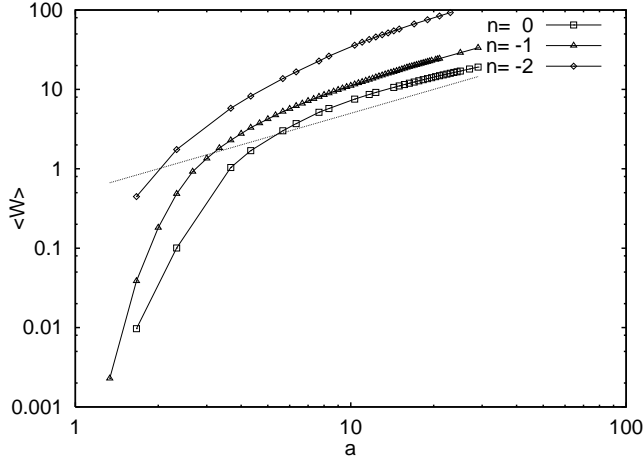


Figure 6. Growth of the velocity deflection measure $\langle W \rangle$ in the model P3M1 for different initial spectra with exponents $n = 0$, $n = -1$ and $n = -2$. The dotted line shows a power law $\langle W \rangle \sim a$.

where ω is the time-averaged rate of change of the deflection angle ω for a particle (the average angular velocity for planar orbits) during the whole simulation (from a_0 to a):

$$\omega = 1/(a - a_0) \int_{a_0}^a \frac{d\phi}{da} da \quad (12)$$

The velocity deflection measure W is, of course, zero for linear motions without the change of direction, but also for the case of strong interactions, when particles are trapped into systems and rotate with constant angular velocities ω_i , $\phi_i = \omega_i a$. In order to describe all particles we use a mean value of this measure $\langle W \rangle$. The growth of this measure in time for our simulations is shown in Fig. 5.

The difference of the mean velocity deflection measure between various models (Fig. 5) is considerably smaller than it was for the mean squared deflections (Fig. 4). The P3M1-model leads the pack as before, with its many-particle version close behind, and the tree-code model has generated similar deflections to the high-resolution AMG1. All other models are relatively quiet.

We studied the $\varepsilon = 0.2$ case in more detail, trying to better understand the source of deflections. We continued the run more deep into the nonlinear times (Fig. 6). We can see that the growth, although rather rapid at the start of the simulation (this rise could be probably explained by non-self-consistent starting conditions), levels off to a power law with the exponent $\alpha \approx 1$. As we have largely eliminated the mean-field effects, we may hope that this exponent tells us that the observed growth of $\langle W \rangle$ is caused by two-body effects.

In order to check if this exponent depends on the large-scale environment we repeated the simulations for the model P3M1 for two more power spectra with the exponents $n = -2$ and $n = 0$. As can be seen from Fig. 6, the deflections grow in a similar fashion, and the exponents are practically

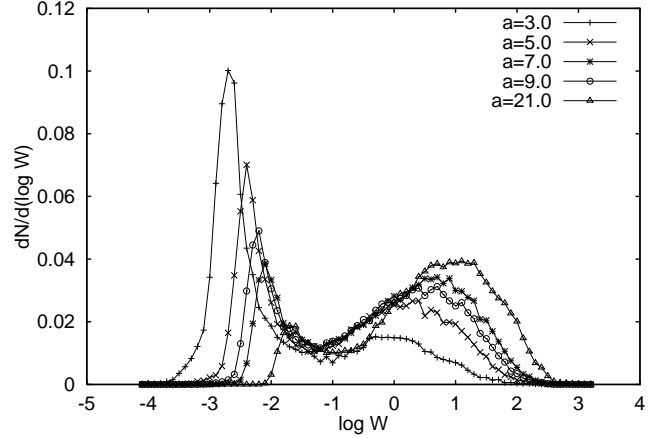


Figure 7. Distribution of the velocity deflection measure W for all particles in the P³M-model P3M1 for different moments a . The signature of high-deflection gravitational collisions is clearly seen as the right maximum. Observe how the distribution that is dominated by small deflections at the start of the simulation shifts gradually over to relatively large deflections.

the same – the curves differ by a multiplicative factor only. Examination of density distributions confirms that structure is much stronger in the $n = -2$ case, the $n = 0$ spectrum giving rise to a large number of small clumps and a rather diffusive sea of particles in between. This will naturally lead to a larger collision rate for the former model.

It is clear that different particles follow extremely different orbits, and in order to understand their evolution it is better to ‘differentiate’ the average quantities shown in Figs. 5-6 and to study the distributions of the velocity deflection measure for our collection of trajectories.

Fig. 7 demonstrates the evolution of this distribution in time for the collisional model P3M1. The main feature of this distribution is the presence of two strong maxima at all times. We may suppose that the left maximum at smaller deflections is describing mean-field effects and the right maximum – gravitational collisions. During the evolution the number of particles that participate in collisions grows steadily. We see also the gradual shift of the distributions towards larger deflections – the accumulated velocity deflections grow. The width of the right maximum that can be thought of as describing the number of strong collisions (about 3 per unit logarithmic interval) grows also.

Similar distributions for the multigrid model AMG1 are shown in Fig. 8. They are distinctly different from the P³M model shown before, having only one small-deflection maximum. During evolution the distribution spreads and only the last distribution that corresponds to highly nonlinear stages of evolution of structure (more than two present lifetimes of the Universe into the future) shows presence of an appreciable high-deflection tail. This tail is caused by the growth of small-scale substructure by far beyond the present epoch.

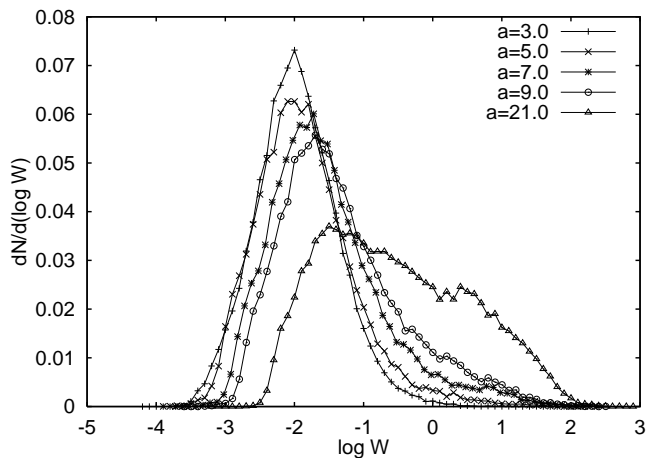


Figure 8. Distribution of the velocity deflection measure W for the multigrid model AMG1 for different moments. The deflection measure grows gradually, but small deflections dominate at all times.

Even more smooth distributions can be found when running the APM model, where the local pairwise forces were ignored. The distributions (Fig. 9) show only the signature of mean-field forces and do not evolve practically at all. This shows, first, a total absence of gravitational collisions typical for its parent P³M-model, but also less substructure than in the AMG1-model (the spatial resolution of the present model was about 4 times lower than that of the AMG1). An exception is the distribution for large times that shows features similar to the AMG1, even with slightly larger amplitudes.

The tree-code shows features in between of the P3M1-model and the smooth models – the distribution of the velocity deflection measure W (Fig. 10) is rather wide, comparable to that of the model P3M1, but it has only one maximum at all times. As the transformation between the physical time coordinate t used here and the ‘scale factor time’ a used for other models is nonlinear, it is difficult to compare these distributions directly with the W -distributions for other models. Even the strong-field approximations (10) do not agree with each other, and the measure W here implies a non-constant mean angular velocity in a .

As we saw above, the overall growth of the deflection measure was similar for our multigrid models and for the P³M-models with rather large softening parameters (Fig. 4). The comparison of the distributions of the velocity deflection measure W at the end of the simulations, $a = 9$ for the P³M-models with different softening is shown in Fig. 11. Only the standard model P3M1 ($\varepsilon = 0.2$) shows a strong collision signature, for the smooth model P3M2 ($\varepsilon = 1$) the right maximum is already very weak and the ‘oversmoothed’ P3M3 ($\varepsilon = 2$) shows only mean-field deflections. It is even smoother than the APM-model, where the local pairwise interactions were ignored. We see also that the models with

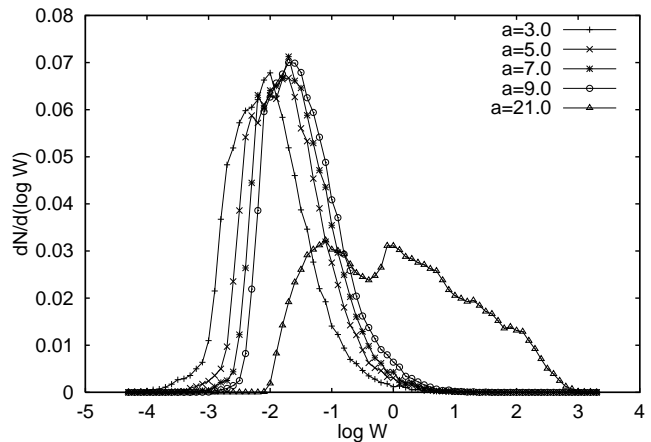


Figure 9. Distribution of the velocity deflection measure W for the APM-model (without local forces) at different times. The distribution is initially smoother than for the multigrid models in Fig. 8, and the final highly nonlinear stage develops similar fluctuations.

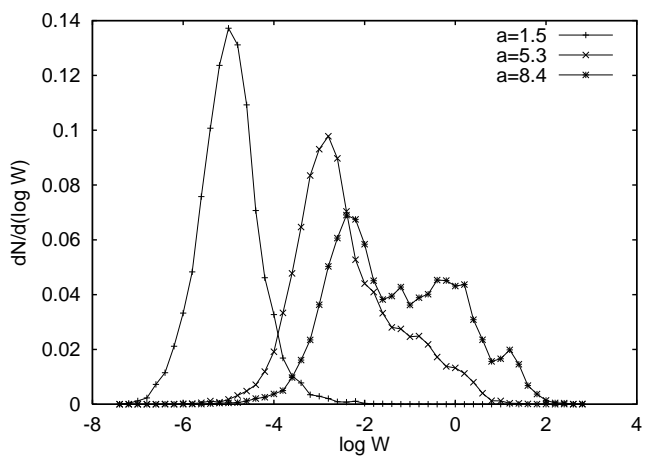


Figure 10. Distribution of the velocity deflection measure W for the tree-code simulation at different times. The distribution is rather wide, but has only one maximum at all times.

a large softening develop much smaller accumulated deflections.

The deflection characteristics we have studied so far have all been accumulated from the start of the simulation. As the deflection angle is positively defined, the change of its mean value, describing smooth-field effects, will contribute

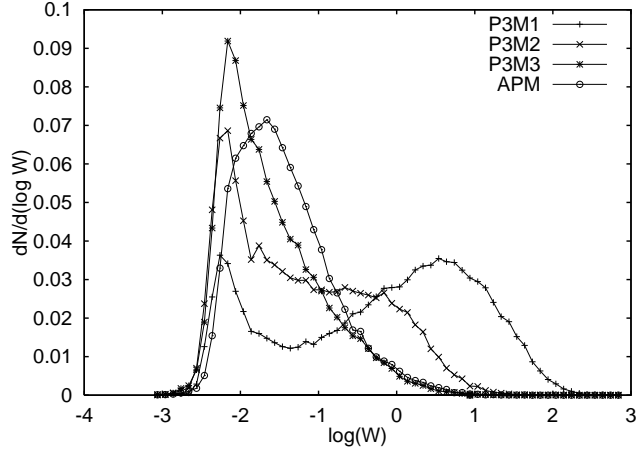


Figure 11. Distribution of the velocity deflection measure W at the final stage of simulations for P³M-models with different softening parameters. The role of collisions (the right maximum) decreases rapidly with a growing ε .

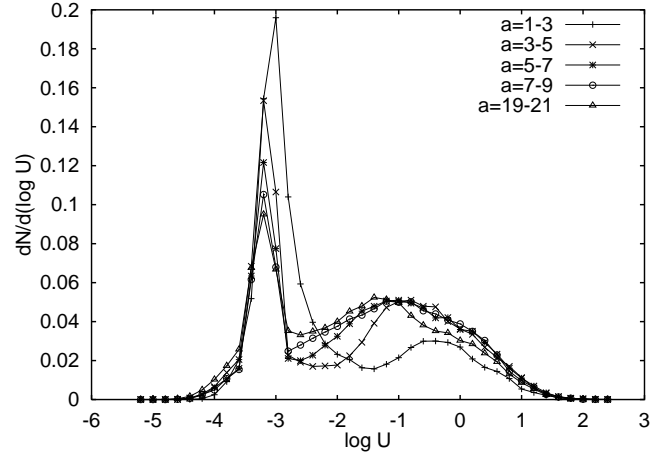


Figure 13. Distributions of the deflection rate U for the P³M-model P3M1 for different time intervals. The left maximum describes the mean-field effects while the right maximum describing collisions grows steadily.

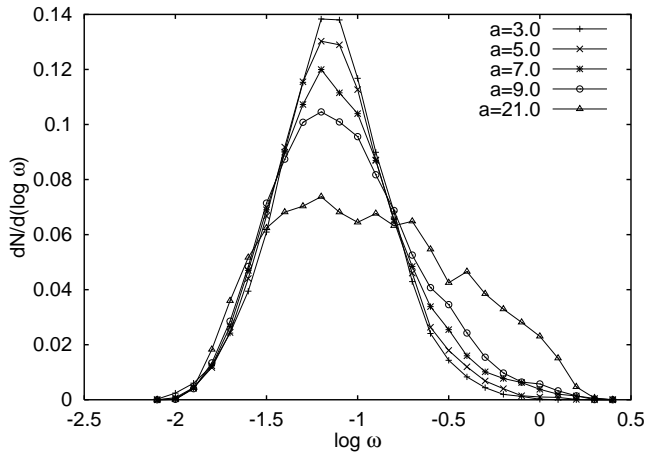


Figure 12. Distribution of the mean angular velocity ω for different moments (the model AMG1). The initially concentrated distribution spreads in time both due to collisions and mean-field effects.

in some extent to the velocity deflection parameter W . We show a typical distribution of ω in Fig. 12 for the model AMG1. Its time dependence is rather slow, but ω tends to grow, and this may influence the accumulated velocity deflections.

In order to eliminate this effect, we performed another step of ‘differentiation’, separating the overall evolution into a number of time intervals $a \in [a_i, a_{i+1}]$ and calculating the rate of growth of the velocity deflection measure (deflection rate) U by

$$U = W(a_i, a_{i+1}) / (a_{i+1} - a_i), \quad (13)$$

where $W(a_i, a_{i+1})$ is the same expression as in (11,12) but we have changed the integration limits from (a_0, a) to (a_i, a_{i+1}) . It is important to keep in mind that this operation does not subtract distributions at different times, we differentiate along the accumulated angular velocity deflections.

In Fig. 13 we see again the results for the P3M1-simulation. The picture is essentially the same as in Figure 7. Only the distributions for different times are more similar, and the roles of small deflections for a subinterval (mean-field effects) and those of large deflections are more clearly separated. The small-scale peaks do not move, indicating that the mean-field effects stay the same during the evolution. We built a similar graph for the model P3M4 that differs from the present model only by a larger number of particles. As suggested by a similar behaviour of the deflection measure S (see Fig. 4) the distributions are practically the same.

The distributions of the deflection rate in the adaptive multigrid code are shown in Fig. 14. The figure reveals a noticeable difference between the U -distribution from the first and the successive time intervals. A probable reason for this could be a non-self-consistent initial state that gives rise to initial transients (such transients were observed also by Hernquist & Barnes, 1990, in their analysis of tree-code models). This could be caused by the presence of softening in the force law as supposed by Hernquist & Barnes. Models

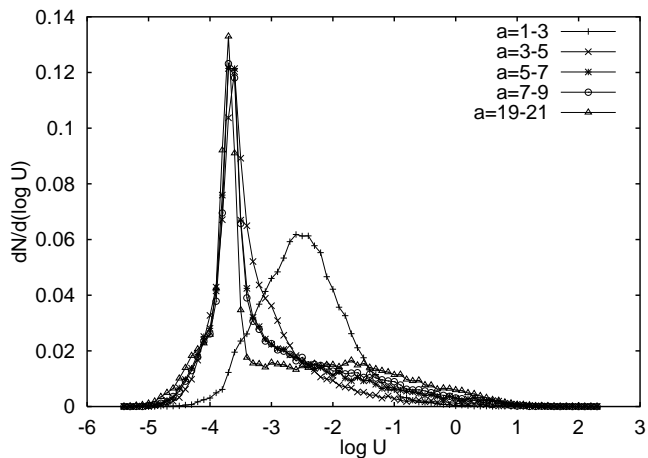


Figure 14. Distributions of the deflection rate U for the multi-grid model AMG1. After the initial fast evolution towards a quasiequilibrium growth, most particles keep moving smoothly and only a small percentage of them suffers deflections that place them in the high-deflection tail of the distribution.

evolve rapidly away from this stage, but they acquire in the process a high-deflection tail of the distribution of the deflection measures. The later evolution is much more quiet, with most of the deflections coming from small-amplitude mean-field accelerations. At later times yet when higher resolution grids are used we see also a growth of the high-deflection tail. This could be partly a mean-field effect and could be partly caused by force errors. This tail is, however, much lower than that for the P3M1-model and there is no sign of any maximum. This figure also shows that the strong difference between the W -distribution for nonlinear stages (see Fig. 8) is due to a large difference between the moments they have been constructed, the deflection rate being practically the same at $a = 9$ and at $a = 20$.

It is instructive to compare Fig. 13 with Fig. 15, where the U -distribution from the APM simulation is shown. This shows the difference between trajectories of particles which undergo short-range accelerations and which do not. The APM distribution is in fact very close to that for AMG, but it almost does not have the long high-deflection tail. There are at least two reasons for this – firstly, the adaptive grids in the APM did not reach as deep as they did in the AMG-models, and secondly, the subgrid force calculation procedure used in the AP³M-approach might give cleaner forces.

Extra gravitational collisions inherent to a N -body code can influence directly the conclusions that we make comparing our models to observations. As they generate additional velocity changes, their presence is reflected most clearly in the velocity distributions. These can be compared easily with observations and they influence the properties of the gravitationally bound systems that are born during the

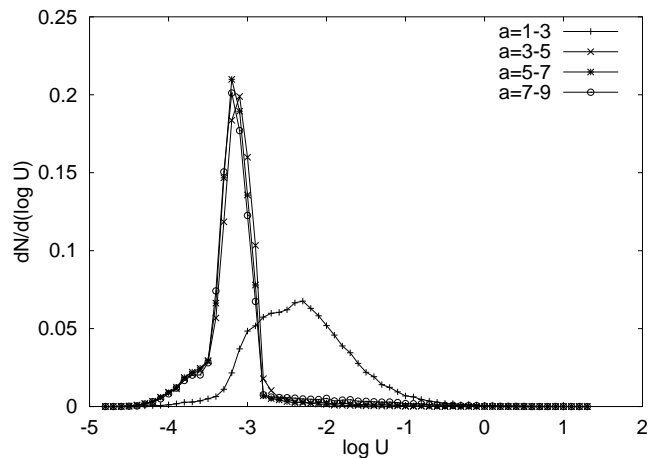


Figure 15. Distributions of the deflection rate U for the APM-model. Here one observes only the initial fast relaxation, but there are practically no collision events.

simulations. As an example, we analyzed the distributions of relative velocities for particle pairs for different codes.

The relative velocity vector between a pair of particles can be decomposed into the line-of-sight (‘radial’) component and into the component perpendicular to this direction (‘tangential’) (see Gelb 1992). The radial component v_{\parallel} can be defined as

$$v_{\parallel} = \frac{(\mathbf{v}_1 - \mathbf{v}_2) \cdot (\mathbf{x}_1 - \mathbf{x}_2)}{|\mathbf{x}_1 - \mathbf{x}_2|} \quad (14)$$

and the perpendicular velocity component v_{\perp} as

$$v_{\perp} = ((\mathbf{v}_1 - \mathbf{v}_2)^2 - v_{\parallel}^2)^{1/2}. \quad (15)$$

The dispersions of these velocities are shown in Fig. 16 for the final moment $a = 9$, corresponding roughly to the present epoch, for three different models, P3M1, AMG1 and APM. This figure shows that the P³M-code gives velocity dispersions that are about 50% larger than we get using smooth-field codes to model the same patch of the Universe. The results we have seen above let us suspect that this difference may be mainly due to two-body effects in the P³M-code. And as we already mentioned, this could affect the conclusions one makes about the rotation velocities and masses of the systems that form and about the ease they form with.

4 CONCLUSIONS

We have compared a range of P³M-models with different softening parameters and spectra and smooth-density models of comparable spatial resolution (APM, multigrid). We have seen that smooth-field PM-codes are considerably less collisional than the P³M-codes. We have found that even choosing comoving softening parameters instead of physical

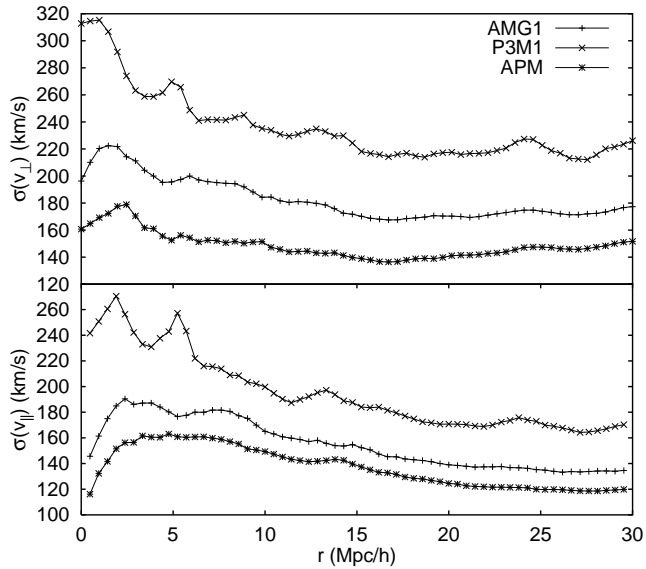


Figure 16. Dependence of the pairwise longitudinal (“radial”) velocity dispersion $\sigma(v_{\parallel})$ (panel a) and the transversal velocity dispersion (“rotation velocities”) $\sigma(v_{\perp})$ on the width of particle pairs r for different models. We see that the dispersion obtained from the P³M-models is much larger than that from the smooth models, even at relatively large distances.

ones there is a considerable amount of gravitational collisions in standard P³M-models. If their influence is crucial for the problem the simulation is run for (e.g. the study of velocity dispersions or of the formation of bound systems), we would recommend to use comoving softening parameters $\epsilon \geq 1.0$.

We have also proposed a new approach to study gravitational collisions in nonstationary systems that are common in cosmological simulations. We use measures based on the accumulated deflection angles of particle orbits and on accumulated angular velocity deflections. These measures are similar to the commonly used energy diffusion and orbit divergence measures, but they do not saturate during evolution.

ACKNOWLEDGEMENTS

Our special thanks go to Dr. H. Couchman who sent us his AP³M code that was one of the two workhorses for this study. We thank Dr. J. Peacock for suggesting the subinterval analysis for the deflection velocity distributions that made the picture much clearer. We are much indebted to Dr. B. Jones for the discussion of the paper. IS thanks the Edinburgh Observatory and the Edinburgh Parallel Computing Centre, where most of the simulations for this work were done, and both of us thank the new Theoretical Astrophysics Center in Copenhagen, where the article was finished, for supporting our stay there. IS was supported in Edinburgh by the EC TRACS scheme and both authors were supported by the Estonian Science Foundation grant 338.

REFERENCES

- Anninos P., Norman M.L., Clarke D.A., 1994, *ApJ*, 436, 11
 Bagla J.S., Padmanabhan T., 1995, *astro-ph* 9503121
 Barnes J.E., Hut P., 1986, *Nature*, 324, 446
 Brandt A., 1984, *Multigrid Techniques: 1984 Guide with Applications to Fluid Dynamics*. GMD-Studien 85, Bonn
 Brandt A., 1977, *Math. Comput.*, 31, 333
 Couchman H.M.P., 1991, *ApJ*, 388, L23
 Couchman, H.M.P., 1995, in *Numerical Methods in Astrophysics*, Springer, N-Y (in press)
 Gelb J.M., 1992, MIT Ph.D. thesis
 Gelb J.M., Bertschinger E., 1994, *ApJ*, 436, 467
 Hackbusch W., 1985, *Multi-Grid Methods and Applications*, Springer, N-Y
 Hernquist, L., Barnes J.E., 1990, *ApJ*, 349, 562
 Hockney R.W., Eastwood J.W., 1988, *Computer simulation using particles*, IOP, Bristol
 Huang S., Dubinski J., Carlberg R.G., 1993, *ApJ*, 404, 73
 Jessop R.S., Duncan M., Smith E., 1994, *J. Comp. Phys.*, 24, 666
 Pen U-L., 1994, Princeton University Observatory Preprint
 Splinter R.J., 1995, *astro-ph* 9503041
 Standish E., Aksnes K., 1969, *ApJ*, 158, 519
 Suisalu I., Saar E., 1955, *MN*, 274, 287